Submitted to Journal of Nanoscience and Nanotechnology

Final Version

Submitted: January 04, 2010
Revised/Accepted: February 08, 2010

Thermal and Rheological Properties of Biodegradable Poly[(butylene succinate)-co-adipate] Nanocomposites

Jayita Bandyopadhyay,[1] Arjun Maity,[1] Bhanu Bhusan Khatua,[2] and Suprakas Sinha Ray[1, 3] *

[1]*DST/CSIR Nanotechnology Innovation Centre, National Centre for Nano-Structured Materials, Council for Scientific and Industrial Research, Pretoria 0001, Republic of South Africa.*

[2]*Materials Science Centre, Indian Institute of Technology, Kharagpur, Kharagpur 721302, India*

[3]*Department of Chemistry, Faculty of Natural and Agricultural Sciences, University of the Free State (Qwaqwa Campus), Phuthaditjhaba 9866, Republic of South Africa.*

The thermal and rheological properties of clay-containing poly[(butylene succinate)-co-adipate] (PBSA) nanocomposites are reported. The nanocomposites of PBSA with various weight percentages of organically modified montmorillonite (OMMT) loadings have been prepared by melt-mixing in a batch-mixer. The melting and crystallization behaviours of PBSA and its nanocomposites have been studied using differential scanning calorimeter (DSC). The melt-state rheological properties of pure PBSA and its nanocomposites containing different amounts of OMMT have been studied in detail. The reason for this is that the rheological responses of any nanofilled polymeric materials are strongly related by their dispersed structure and the interfacial characteristic. Results show that the structural strength of all samples remains constant in the examined time interval at an experimental temperature. The dominant viscous behaviour of pure PBSA is getting suppressed up to a certain OMMT loading (4 wt.%). Nanocomposite containing 5 wt.% OMMT is showing almost "at the gel point" behaviour, suggesting that the material is behaving near the borderline between liquid and solid; while nanocomposite containing 6 wt.% OMMT is showing the gel character. The dispersed structure of the clay particles in the PBSA matrix was studied by scanning transmission electron microscopy (STEM). Results show that the stacked and intercalated silicate layers are nicely dispersed in the case of all nanocomposites. However, with a systematic increase in OMMT loading, the dispersed clay structure of the nanocomposites changes from a highly delaminated to a flocculated and then to a stacked-intercalated structure. In the case of all nanocomposites, melt–state rheological properties are in good agreement with the STEM observations.

Keywords: Poly[(butylenes succinate)-co-adipate]; Nanocomposites; Thermal and rheological properties.

* To whom all correspondences should be addressed. E-mail: rsuprakas@csir.co.za

1. INTRODUCTION

In recent years, a great effort has been made to develop high-performance novel polymeric materials through the benefit of nanotechnology. One of such niche areas is polymer nanocomposite (PNC) technology.[1-15] By definition, PNCs are really nanofilled plastics, where the total interfacial area becomes th critical characteristic rather than simply the relative volume fraction of constituents. However, the use of the term PNCs invokes parallels to the traditional fiber-reinforced composite technology and the ability to spatially 'engineer, design, and tailor' materials performance for a given application.[16] Recently, PNC technology not only expands the performance space of traditional filled polymers, but also introduces completely new combinations of properties and thus enables new applications for plastics. [1, 17, 18]

Of particular interest is the clay-containing PNC that consists of a polymer and pristine or organically modified clay which often exhibit concurrent improved properties as compared to those of the pure polymer.[19–28] In general, it is believed that these concurrent property improvements in polymer/clay nanocomposite come from the interfacial interactions between the polymer matrix and the clay particles, as opposed to the conventional composites.[18] The clay particles have a layer thickness on the order of ~1 nm and a very high aspect ratio (10–1000). A few weight percent (~5 wt.%) of clay, which are well dispersed throughout the polymer matrix, thus create much more surface area for polymer/filler interactions than do conventional composites. In the case of PNC, the lower loadings also facilitate processing and reduce component weight. However, the most important feature of PNC is the unique value-added properties not normally possible with traditional fillers such as reduced permeability, optical clarity, self-passivation, and increased resistance to oxidation and ablation.[24, 25] Over the last few years, nearly all types of polymer matrices have been used for the preparation of nanocomposites with both pristine and organically modified clays, and research efforts have produced many interesting results, including some commercial products. [24, 25]

PBSA is a synthetic aliphatic polyester and is synthesized by the polycondensation of butane-1,4-diol in the presence of succinic and adipic acids with relatively low production cost and satisfactory mechanical properties equivalent to that of polyolefins.[29–31] The molecular structure of PBSA is presented in **Scheme 1**. PBSA, compared with poly(butylene succinate), is more susceptible to biodegradation because of its lower crystallinity and more flexible polymer chains.[31] It also has excellent processability, so that it can be processed in the field of textiles into melt blow, multifilament, monofilament, flat, and split yarn, and also in the field of plastics into injection moulded products. It is, thus, a promising polymer for various applications.

$$[\text{-O-}\{(CH_2)_4\text{-O}\}\text{-}\{\text{CO-}(CH_2)_2\text{-CO-}\}_x\text{-}\{\text{CO-}(CH_2)_4\text{-CO-}\}_y\text{-}] \qquad x+y=1$$

Scheme 1. The molecular structure of poly[(butylene succinate)-co-adipate] (PBSA).

In our recent publications in this series, [32–36] we have reported on the preparation, characterization, and mechanical, thermal, and rheological properties of various types of PBSA nanocomposites prepared with different types of organically modified clays. In all cases the intrinsic properties of the neat PBSA are concurrently improved after nanocomposites formation. The effect of incorporation of organoclay on the non-isothermal crystallization behaviour, kinetics, and finally, cold crystallization

behaviour of PBSA have also been studied. [37–38] Results showed that the incorporation of organoclay decelerates the crystallization kinetics and slowdown the crystal growth of PBSA. This was attributed to the homogeneous dispersion of the silicate layers into the PBSA matrix.

The main objective of this work is to report the thermal and melt-state rheological properties of PBSA/OMMT nanocomposites in detail. A series of PBSA nanocomposites with various amounts of OMMT, such as from 0.2 – 9 wt.%, were prepared and the rheological properties were studied in detail. This was done because the rheological responses of clay-containing polymer nanocomposites are strongly influenced by their nanostructure and the interfacial characteristics. Finally, nanocomposite structures were analyzed by high-resolution scanning transmission electron microscope (STEM).

2. EXPERIMENTAL PART

2.1. Materials

PBSA used in this study is a commercial product from Showa High Polymer (Japan), with the designation BIONOLLE # 3001, which according to the supplier has a weight average molecular weight, M_w = 190 kg/mol, specific gravity = 1.23 g/cm^3 (ASTMD729), and melt flow index (MFI) = 1.8 gm/10 min (190°C, ASTM1238). The molar ratio of succinate unit to the adipate unit is ~ 4:1 and the content of the coupling agent (hexamethylene diisocyanate) unit is ~0.5 mol.%. Organoclay used in this study was Cloisite®30B (C30B), purchased from the Southern Clay Products, USA. According to the supplier, the pristine MMT is modified with 30 wt.% of methyl tallow bis(2-hydroxylethyl) quaternary ammonium salt. The reason for choosing C30B as an OMMT in this study is that it has the closest value of the polar solubility parameter of the surfactant (21.5 J$^{1/2}$.cm$^{-3/2}$) with that of PBSA (23.8 J$^{1/2}$.cm$^{-3/2}$). [39] Prior to melt blending, the polymer was dried under vacuum at 60ºC for 48h and C30B at 75ºC for 4h. The molecular structure of the surfactant used to modify pristine MMT is shown in Scheme 2.

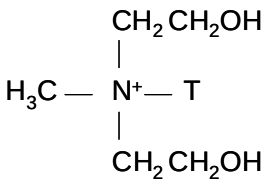

Scheme 2. Chemical structure of bis(2-hydroxylethyl) quaternary ammonium. ‘T’ represents tallow (~65% C18; ~30% C16; ~5% C14).

2.2. Nanocomposite Preparation

Since PBSA is a semicrystalline polymer having the highest melting peak temperature at around 95ºC, the selected processing temperature was 125ºC. Nanocomposites of PBSA with various C30B loading were prepared via melt-mixing technique. PBSA was first melted in a Polylab Thermohaake-batch mixer at 125°C (set temperature) for 1.5 min with a rotor speed of 60 rpm. C30B powder was then

added for 1 min and blended for 6.5 min. The dried nanocomposite strands were converted into sheets with a thickness of 0.4–1.5 mm by pressing with 2 torr pressure at 125°C for 2 min using the Craver Laboratory Press. The PBSA nanocomposites with various wt.% of C30B such as 0.2, 0.5, 1, 1.5, 2, 2.5, 3, 4, 5, 6, 9, were correspondingly abbreviated as PBSANC0.2, PBSANC0.5, PBSANC1, PBSANC1.5, PBSANC2, PBSANC2.5, PBSANC3, PBSANC4, PBSANC5, PBSANC6, and PBSANC9.

2.3. Characterizations

Melting and crystallization behaviours of pure PBSA and nanocomposite samples were studied on a TA Instruments (DSC model Q2000 series) under constant nitrogen flow of 50 ml/min. DSC samples were weighed such that all samples had identical PBSA content. The sample weight was maintained between 10-10.9 mg depending on the clay loading. The temperature and the heat of fusion were calibrated with an indium standard, and the baseline was checked according to TA Instruments protocols. After equilibration at -75ºC for 20 min, the samples were heated to 135ºC at a rate of 20ºC/min; kept at this temperature for 5 min to destroy any previous thermal history; then cooled down to -75ºC at a cooling rate of 20ºC/min and again heated to 135ºC at a rate 20ºC/min as soon as cooling was finished.

The thermal stabilities of the pure polymer and the C30B powder were investigated by thermogravimetric analyzer (TGA, TA Instrument TGA Q500 model), under air atmosphere. The samples were heated to 125ºC at a rate of 20ºC/min, kept at that temperature for 15 min, and then heated to 700ºC at a ramp rate of 20ºC/min. From TGA scans, it is clear that there are only 0.4 and 1.1 percent (this is due to adsorbed water) weight loss for PBSA and C30B, respectively, at the processing temperature of 125°C after 18 min. The change of mass and derivative weight loss throughout the temperature range was also examined. PBSA shows one pronounced degradation step with a little hump; whereas C30B shows two steps degradation.

The flow behaviour of pure PBSA and various nanocomposites in both melt and solid states were studied by an Anton-Paar stress-strain controlled rheometer model MCR-501 with parallel plate (PP-25) configuration and solid rectangular fixture (SRF), respectively. To do the dynamic oscillatory measurements one should first determine the amplitude of oscillation in the linear viscoelastic (LVE) region where any structural change is supposed to be reversible. Hence, the strain amplitude sweep experiments of all samples were performed at 125ºC with a constant angular frequency (ω) = 6.28 rad/s in the varying strain window 0.01 – 100%. The frequency sweep experiments were carried out at the same temperature with a strain amplitude of 0.1% in the frequency rage 100 – 0.01 rad/s. For time sweep experiments, the samples were investigated for 1200s at a constant temperature of 125ºC, strain = 0.1% and ω = 6.28 rad/s.

The degree of dispersion of silicate layers in the PBSA matrix was evaluated by STEM. For the STEM studies, ~75 nm thick compression moulded nanocomposite lamellae were prepared using a Focused Ion Beam FEI Helios Nanolab SEM (FIB-SEM) (Gallium ion source and beam current was 0.92 mA), operated at 30 kV. To avoid damage, the sample surface was first covered with a platinum deposition. Details regarding lamella preparation by FIB-SEM can be found elsewhere.[35] Bright-field STEM images of various nanocomposite samples were taken in a FEI Helios Nanolab SEM using STEM-II detector.

3. RESULTS AND DISCUSSION

3.1. Effect of C30B Loading on the Melting and Crystallization Behaviours of Pure PBSA

To understand the effect of C30B incorporation on the melting and crystallization behaviours of pure PBSA, all samples were examined by DSC according to the conditions described in the characterization section. DSC scans of various samples are presented in **Fig. 1**, and results are summarized in **Table 1**. The glass transition temperature (T_g) of pure PBSA is clearly visible in the first heating cycle and not systematically; however, T_g of PBSA slightly increases with the addition of C30B (refer Figs. 1a & 1a′, Table 1). In the first heating cycle, all samples show three-step melting behaviours with some extent of recrystallization phenomena just before the third melting. On the other hand, in the second heating scan, all samples melt in two steps with one pronounced recrystallization step in between (refer Figs. 1b & 1b′, Table 1). During first heating, the first melting peak (T_{m1}) of nanocomposites appears almost at the same temperature as PBSA, whereas the second melting peak (T_{m2}) moves towards the higher temperature region with respect to the pure PBSA with increase in C30B loading up to 2 wt.%. Not systematically, however, the value of T_{m2} starts to decrease with further C30B loading. On the other hand, the value of T_{m3} of PBSA systematically decreases with C30B loading.

The incorporation of clay does not affect the onset crystallization temperature of PBSA ($T_{c\ on}$) significantly; however, the crystallization peak temperature (T_c) moves to the lower temperature with increase in C30B loading (refer Figs. 1c & 1c′, Table 1). The enthalpy of crystallization (ΔH_c) also shows almost the same trend as observed in the case of T_c. However, the onset of melting temperature ($T_{m\ on}$) of pure PBSA during second heating increases with C30B loading. With the addition of a very small amount of C30B (~4 wt.%), both melting peaks of nanocomposites shift to the lower temperature region, but there is no significant change with further increase of C30B content. On the other hand, the total enthalpy of fusion (ΔH_f) of two melting peaks of PBSA remains almost constant up to 1.5 wt.% of C30B loading; and then decreases with further C30B loading.

For the semicrystalline polymers, in the glass transition region, the strong interaction forces contributed by the crystalline phase prevents polymer chains from gliding on each other and the amorphous portion starts melting which results in a softer consistency due to the increase in mobility. In the case of nanocomposites, the high degree of dispersion of silicate layers in the PBSA matrix hinders the gliding ability and hence T_g of PBSA matrix slightly increases in nanocomposites. The appearance of three melting peaks of PBSA matrix in the first heating cycle is probably due to the presence of different sizes of PBSA crystals distribution.[34] First, the small size crystals undergo melting and then larger ones with some recrystallization. This exothermic recrystallization could be due to either growth of crystals after softening or some rearrangement of crystals during melting. At the end of melting, samples attain isotropization and consequent cooling results in crystals growth. It is well known that the incorporation of any foreign material in the polymer matrix usually acts as a nucleating agent to start this crystallization growth mechanism. According to **Table 1**, the nucleation efficiency of C30B (determine by $T_{c\ on}$) is not so pronounced. As long as the C30B content is very low (up to 1 wt.%), the dispersed silicate particles facilitate the nucleation and growth process (reflected by higher $T_{c\ on}$ compared to polymer). However, in the case of nanocomposites with higher C30B loading because of the high level of dispersion of silicate layers, the PBSA crystals growth get hampered and hence T_c shifts towards the lower temperature with a decreased value of ΔH_c. The increasing trend of $T_{m,\ on}$ (refer **Table 1**) with increase in C30B loading in nanocomposites suggests that the thermal stability of PBSA crystals against melting is improving in the presence of clay

particles. The reason of the appearance of two melting peaks during the second heating cycle instead of three as observed in first heating scan is due to the formation of more perfect PBSA crystals during crystallization from melt.[34] The value of T_{m2} and T_{m3} (from the second heating scan) remains the same as T_{m2} and T_{m3} (from the first heating scan) for all nanocomposites. Since the crystals that grow during cooling undergo melting, the decreasing trend of ΔH_f values with an increase in clay loading also confirms that the crystal growth is hindered by the presence of highly dispersed clay layers and hence nanocomposite samples show lower melting temperatures relative to the pure polymer during second heating.

3.2. Melt-state Rheological Properties

The behaviour of polymeric materials is based on the combination of both the viscous and the elastic portions, and therefore, they are known as viscoelastic material. The rheological experiments in molten states reveal information about the flow behaviour of such materials since any large deformation produced by shear forces cause polymeric materials to flow. This work focuses mainly on the flow behaviours of the pure PBSA and PBSANCs due to the applied oscillatory shear flow.

3.2.1. Amplitude Sweeps

For any oscillatory test it is necessary to determine the amplitude of oscillation for which any structural modification is reversible. To find out this reversible region, the strain amplitude sweep experiments were performed at 125ºC with a constant angular frequency, ω = 6.28 rad/s in the varying strain of 0.01 – 100%. The temperature was selected in such a way that there is no degradation of PBSA matrix as checked by TGA and the samples are in an isotropic phase. Therefore, any structural change in this state is the result of applied shearing force. As demonstrated in **Fig. 2** for all samples at low amplitude values in the so-called linear viscoelastic (LVE) region, both the storage modulus, G' (representing the elastic behaviour) and loss modulus, G'' (representing the viscous behaviour) are showing constant plateau values. **Fig. 2** also shows that the pure PBSA has liquid / sol character in the entire amplitude range since G'' is dominating over G'. With increase in C30B loading in the PBSA matrix results in improvement of G' over G'' and the difference in level of G' and G'' plateau are getting closer. In the case of PBSANC5, G' plateau is nearly overlapping on G'' plateau. On the other hand, in the case of both PBSANC6 and PBSANC9, there is a crossover point where $G' = G''$, then the liquid character with $G' < G''$ changes to gel character with $G' > G''$. The parameters γ_L and γ_F, reported in **Table 2**, respectively, representing the yield strain of the LVE range, i.e. the point from where the LVE plateau starts to deviate noticeably and the flow point where $G' = G''$ and the region between γ_L and γ_F is known as yield zone. Thus, the strain chosen for the other oscillatory tests is 0.1%, which makes it possible to study the material behaviour in the LVE region.

PBSA is showing viscous behaviour, similar to liquid, and thus easy to flow. In the case of nanocomposites probably the cross-linked network starts to form after the incorporation of C30B and hence, the elastic property is improving with the increase in C30B loading. This can be confirmed by the frequency sweep results. From the γ_L and γ_F values (refer **Table 2**) it is clear that the network structure of the nanocomposites are changing significantly from PBSANC4 to PBSANC5 and then in the case of PBSANC5 to PBSANC6. Therefore, the percolation threshold value for rheological properties of nanocomposites lies between 4 to 6 wt.% of C30B.

3.3.2. Frequency Sweeps

Frequency sweep results are useful to investigate the time-dependent shear behaviour since the frequency is the inverse value of the time. Short-term behaviour is simulated by the rapid motion (i.e., at high frequencies) and long-term behaviour by slow motion (*i.e.,* at low frequencies). The frequency dependent response of PBSA and PBSANCs are presented in **Fig. 3**. In the higher frequency region, all samples show $G' > G''$. After a certain frequency (~1 rad/s) PBSA and PBSANCs up to 4 wt.% C30B loading show $G' < G''$. For PBSANC5 there is a frequency region where both moduli are overlapping and in the very low frequency region it is nearly approaching a constant limiting value. Further increase in C30B loading results enhance G' more than G'' in the entire frequency range examined with constant limiting value (for better understanding see **Fig. 4**). According to **Fig. 3c**, the complex viscosity, $|\eta^*|$ of pure PBSA increases with a decrease in frequency and approaches nearly a zero shear viscosity value. The PNBSNCs with C30B loading from 0.2 – 3 wt.% (PBSANC0.2 to PBSANC3) are also showing the same trend like pure PBSA. In the case of PBSANC4, instead of attaining a zero shear viscosity plateau, the viscosity increases slightly and hence the steepness of the curve increases compared to PBSANC3. A sudden change in viscosity can be observed for PBSANC5. With further increase in C30B loading, $|\eta^*|$ increases systematically as angular frequency decreases. Like amplitude sweeps, a dramatic change in viscoelastic properties can be observed in PBSANC3 to PBSANC4, then to PBSANC5 and PBSANC6. Therefore, these four nanocomposites along with PBSA are considered as model systems to understand the structure-property relationship in detail.

Now the nature of the frequency sweep curves can be explained in the following way:[40]

In general, $|\eta^*| = \eta' - i\eta''$ (2)

where, the real part of complex viscosity, $\eta' = \frac{G''}{\omega}$ (3)

and the imaginary part of complex viscosity $\eta'' = \frac{G'}{\omega}$ (4)

Therefore, the elastic behaviours are determined in terms of G' and η'' and viscous behaviours by G'' and η'. **Figs. 4** a & b show initially $G' > G''$ in the high frequency region for all samples. Such an observation indicates that with an increase in ω, G' increases, or in other words, according to equation (4), η'' increases and hence, $|\eta^*|$ decreases. Physically, one can think that during the faster motion, the polymer structures of temporary entanglements are showing more and more inflexibility and rigidity. In this state more deformation energy can be stored and the loss of deformation energy by friction between polymer chains due to their relative motion gets reduced. Thus, the elastic behaviour is showing increasing dominance with an increase in ω. On the other hand, with a decrease in ω, the network of entanglements gets enough time to start disentangle and hence nanocomposite samples are showing more and more flexibility and mobility. After that, most of the deformation energy is lost by the frictional heating effects between the polymer chains due to their mutual relative motion.[40]

From the steeply falling nature of G' and G'', especially in the low frequency region [see **Figs. 3a & b**], one can say that the pure PBSA and PBSANCs up to 4 wt.% of C30B loading have an unlinked structure, where only mechanical interactions or entanglements are present. The cross-linking makes it impossible for the polymer chains to glide along each other without destruction of their chemical network. Maximum deformation is possible for widely meshed networks. For a closely packed network system a minimum deformation is permissible and hence in the very low frequency region it is expected that the steeply falling nature of moduli should attain a plateau value. Therefore, it can be

confirmed that in the case of PBSANC5 the cross-linking, i.e., the formation of a network between macromolecules that are fixed either by chemical (primary valence bonds forming a chemical network) bonds or by physical-chemical bonds (secondary bonds forming a network of forces) starts. This cross-linking increases with further increase in C30B loading and as a result, G' starts to dominate over G'' in the whole frequency range examined.

Again, the horizontal and vertical shifts of the crossover point, i.e., $G' = G''$, give information about the molar mass and the molar mass distribution (MMD), respectively.[40] According to **Table 3,** the crossover point shifts suddenly towards the lower frequency region in the case of PBSANC3, whereas the crossover point remains the same in the case of PBSANC4 and then again moves to the lower frequency region in the case of PBSANC5. However, PBSANC6 and PBSANC9 do not have any crossover point. For two polymers having the same average molar mass but different MMDs, the polymer possesses wider MMD if the crossover point shifts vertically to the lower G value. Now if the MMDs are the same but molar masses are different, then for the polymer with higher average molar mass the crossover point shifts to the lower frequency value. Therefore, it can be concluded, PBSANC4 has the same average molar mass like PBSANC3 but much wider MMD, and in the case of PBSANC5 both the average molar mass and MMD are changing. It could be the average molar mass is increasing in PBSANC5 due to the cross-linking since $G' = G''$ point shifts towards the lower ω value and as a result it shows inflexibility or less mobility in the lower frequency region. The disappearance of a crossover point in the case of PBSANC6 and PBSANC9 confirms cross-linking increases with C30B loading. Therefore, there will be a significant change in rheological properties in the case of PBSANCs with C30B loading varying from 3 to 6 wt.%. Hence, they are chosen as model systems for further characterization.

3.2.3. Time Sweeps

During melt-rheological tests of polymeric materials, it is also important to know the time-dependent behaviour of material at the experimental temperature. Actually, the purpose of this test is to determine whether the structural strength is remaining unchanged or increasing or decreasing with time under isothermal condition. For this reason, the time sweep experiments of pure PBSA and four model nanocomposite samples such as PBSANC3, PBSANC4, PBSANC5, and PBSANC6 were conducted for 1200s at a constant temperature of 125ºC, an applied strain = 0.1% and ω = 6.28 rad/s. The results are summarized in **Fig. 5**. According to the Fig. , the structural strength of all samples remains constant in the examined time interval at 125ºC. The dominant viscous behaviour of pure PBSA is getting suppressed up to C30B loading of 4 wt.%. PBSANC5 is showing almost “at the gel point” behaviour, suggesting that the material is behaving near the borderline between liquid and solid. On the other hand, PBSANC6 is showing the gel character. This change in properties of nanocomposites with different C30B loadings indicates the formation of different types of network structures of dispersed silicate layers in the PBSA matrix. We will confirm this with STEM observations.

3.3. Solid-State Rheological Property and the Enhancement of Modulus

This test is important to understand the temperature-dependent behaviour of the samples at constant dynamic mechanical conditions. The test parameters are summarized in characterization section. All samples, both pure PBSA and PBSANCs, show a sharp glass transition followed by melting. Therefore, the nature of the curves as presented in **Fig. 6** corresponds to the semi-crystalline material. Here, mostly polymer chains are chemically unlinked and show a partially regular super structure;

which in turn is responsible for the formation of some regular tightly packed structures—so called crystalline regions. These crystalline areas are surrounded by the amorphous parts. Now, there are two ways to determine the glass transition temperature. First, by the determination of the first significant modification of sample's structure from the maximum of lost deformation energy (G'' peak) and second, by the determination of the relative maximum value of spent energy from the maximum of ratio of loss to stored deformation energy (i.e., $tan\delta$).[39] The glass transition and the onset of the melting temperature calculated from the data in **Fig. 6** are tabulated in **Table 4**. According to the data in **Table 4**, there is no significant change in T_g of pure PBSA after nanocomposite formation with the different amount of C30B loading. This result is consistent with the data calculated from DSC (see **Table 1**). However, the onset of melting temperature of pure PBSA determined from the G' plots moves towards the higher temperature region in the case of PBSANC3 and remains unchanged with further increase in C30B loading.

Initially, in the solid state the molecules remain immobile. At T_g, on one hand, still strong interaction forces are present in the crystalline region that prevent polymer chains from gliding off each other. On the other hand, the amorphous part starts melting, which results in increased mobility. These two opposite phenomena are responsible for the softer consistency or the glassy state of the material. In the temperature range of -43 (after T_g) – 40°C, all samples show higher G' value than G''. Such an observation indicates that the high degree of crystallinity is present in the samples. In the temperature range of 40–70°C, small crystallites start melting and hence G' shows a decreasing trend. But initially, it does not fall sharply because the mostly ball-shaped crystallites do not disappear all at once. The melting process is developing from the outermost part to the innermost part of the semi-crystalline phase. After ~70°C, the G' values fall sharply because of vigorous melting. The presence of strong interfacial interactions between the polymer chains and the clay surface are responsible for the enhancement in bond formation (i.e., cross-linking) with an increase in clay loading. This structural modification produces a more perfect crystal structure in the case PBSANCs, and, hence, $T_{m,on}$ moves towards the higher temperature region for PBSANCs compared to PBSA.

3.6. Scanning Transmission Electron Microscopy Observations

Finally, to support the above results, the model nanocomposite samples were investigated by STEM because microscopy allows a qualitative understanding of the internal structure through direct visualization. **Fig. 7** shows the high-annular-angle-dark-field STEM (HAAD-STEM) images of various PBSANCs in which white entities represent the dispersed clay layers. The STEM image of PBSANC3 (refer **Fig. 7a)** shows that as a whole the intercalated silicate layers (very few exfoliated) are dispersed nicely in the PBSA matrix and the inter-particle distance is much higher than the other model nanocomposites. Still there is some overlapping of neighboring particles, which increases the stacking of the clay layers. In the case of PBSANC4 (refer **Fig. 7b)**, the dispersion characteristics are almost the same as PBSANC3; however, only the probability of finding neighbors increases. According to the STEM, PBSANC5 has a flocculated structure, **Fig. 7c**. After that, further increase in C30B loading results the formation of stacked-intercalated structure like in the case of PBSANC6 as shown in **Fig. 7d**.

Therefore, the structure of nanocomposites is changing especially from PBSANC4 to PBSANC5 and then in PBSANC6. With increase in C30B loading, clay stacking increases, the flexibility of the samples decreases and they start to behave like solid materials. For this reason, during melt-state rheological property measurement in the linear viscoelastic region, the viscous property of

nanocomposites show dominant nature as long as C30B loading increases up to 4 wt.%. In the case of PBSANC5 because of the formation of flocculated structure, the value of G' is almost equal to G''. However, due to the presence of stacked intercalated silicate layers, PBSANC6 behaves like a solid material with $G' > G''$.

4. CONCLUSIONS

This article explains how the dispersion characteristics of the organically modified clay particles in the polymer matrix affects the thermal properties and flow behaviours of the nanocomposites. The scanning transmission electron microscopy results show that the amount of organoclay loading plays a vital role in controlling the network structure of dispersed silicate layers of nanocomposites as well as the thermal properties and flow behaviours. Results also show that the 5 wt.% of C30B is the percolation value to start the formation of the strong flocculated structure of dispersed silicate layers. For this reason, flow behaviours of nanocomposites suddenly change with further addition of C30B. Therefore, we can control the flocculated structured of dispersed silicate layers in the PBSA matrix and, hence, various properties.

Acknowledgement

The authors would like to thank the CSIR Executive and the DST, South Africa for financial support.

References and Notes

1. S. Pavlidou and C. D. Papaspyrides, *Prog. Polym. Sci.* 33, 1119–1198 **(2009)**.
2. J. Jin, L. Chen, and M. Song, *J. Nanosci. Nanotechnol.* 9, 6453–6459 **(2009)**.
3. H. J. Choi, K. Zhang, S. Y. Park, and B. Y. Lee, *J. Nanosci. Nanotechnol.* 9, 6089–6095 **(2009)**.
4. M. Naffakh, C. Marco, M. A. Gómez, G. Ellis, W. K. Maser, A. Benito, and M. T. Martínez, *J. Nanosci. Nanotechnol.* 9, 6120–6126 **(2009)**.
5. A. Maity and S. Sinha Ray, *J. Nanosci. Nanotechnol.* 9, 5223–5230 **(2009)**.
6. Y. Kim, C.-S. Ha, T. Chang, W.-K. Lee, W. Goh, H. Kim, Y. Ha, and M. Ree, *J. Nanosci. Nanotechnol.* 9, 4633–4643 **(2009)**.
7. S. Augier, S. Coiai, D. Pratelli, L. Conzatti, and E. Passaglia, *J. Nanosci. Nanotechnol.* 9, 4858–4869 **(2009)**.
8. Z. Qiu, S. Zhu, and W. Yang, *J. Nanosci. Nanotechnol.* 9, 4961–4969 **(2009)**.
9. T. R. Hull, A. A. Stec, and S. Nazare, *J. Nanosci. Nanotechnol.* 9, 4478–4486 **(2009)**.
10. A. P. Piedade, J. Nunes, and M. T. Vieira, *J. Nanosci. Nanotechnol.* 9, 3792–3797 **(2009)**.
11. A. L. F. de M. Giraldi, M. T. M. Bizarria, A. A. Silva, C. Mariano, J. I. Velasco, M. A. d'Ávila, and L. H. I. Mei, *J. Nanosci. Nanotechnol.* 9, 3883–3890 **(2009)**.
12. G. Mago, F. T. Fisher, and D. M. Kalyon, *J. Nanosci. Nanotechnol.* 9, 3330–3340 **(2009)**.
13. H. Althues, P. Pötschke, G.-M. Kim, and S. Kaskel, *J. Nanosci. Nanotechnol.* 9, 2739–2745 **(2009)**.
14. Y.-L. Liu, C.-S.Liu, W. H. Chen, S.-Y. Chen, K.-S. Wang, and M.-J. Hwu, *J. Nanosci. Nanotechnol.* 9, 1839–1843 **(2009)**.
15. Q. Zhang, K. Naito, B. Qi, and Y. Kagawa, *J. Nanosci. Nanotechnol.* 9, 209–215 **(2009)**.
16. K. I. Winey and R. A. Vaia, *MRS Bull.* 32, 314–319 **(2007)**.
17. D. L. Hunter, K. W. Kamena, and D. R. Paul, *MRS Bull.* 32, 323–327 (**2007)**.
18. D. R. Paul and L. M. Robeson, *Polymer* 49, 3187–3204 **(2008)**.
19. F. Chivrac, E. Pollet, and L. Averous, *Mater. Sci. Eng.* R67, 1–17 **(2009)**.
20. Y-L. Lu, Z. Li, Z-Z. Yu, M. Tian, L-Q. Zhang, and Y-W. Mai, *Comp. Sci. Tech.* 67, 2903–2913 **(2007)**.
21. Q. Zhou and M. Xanthos, *Polym. Degrad. Stab.* 93, 1450–1459 **(2008)**.
22. M. Biswas and S. Sinha Ray, *Adv. Polym. Sci.* 155, 167–221 **(2001)**.

23. H. Fischer, *Mater. Sci. Eng. C* 23, 763–772 **(2003)**.

24. S. Sinha Ray and M. Okamoto, *Prog. Polym. Sci.* 28, 1539–1641 **(2003)**.

25. S. Sinha Ray and M. Bousmina, *Prog. Mater. Sci.* 50, 962–979 (**2005)**.

26. A. Dasari, Z-Z. Yu, and Y-W. Mai, *Mater. Sci. Eng.* R63, 31–80 **(2009)**.

27. Q-X. Zhang, Z-Z. Yu, M. Yang, J. Ma, Y-W. Mai, *J. Polym. Sci. Polym. Phys.* 41, 2861–2869 **(2003)**.

28. J. Ma, J. Xu, J-H. Ren, Z-Z. Yu, Y-W. Mai, *Polymer* 44, 4619–4624 **(2003)**.

29. D. R. Ishioka, E. Kitakuni, and Y. Ichikawa Y. In: Doi, Y.; Steinbuchel, A. Editor, Aliphatic Polyesters: Bionolle, Biopolymers, Polyesters III. Applications and Commercial Products. Vol. 4, Weinheim: Wiley-VCH Verlag Gmbh; 2002. P. 275.

30. M. S. Nikolic and J. Djonlagic, *Polym. Degrad. Stab.* 74, 263–270 **(2001)**.

31. T. Fujimaki, *Polym. Degrad. Stab.* 59, 209–214 **(1998)**.

32. S. Sinha Ray and M. Bousmina, *Polymer* 46, 12430–12439 **(2005)**.

33. S. Sinha Ray and M. Bousmina, *Macromol. Mater. Eng.* 290, 759–768 **(2005)**.

34. S. Sinha Ray, J. Bandyopadhyay, and M. Bousmina, *Polym. Degb. Stab.* 92, 802–812 **(2007)**.

35. S. Sinha Ray, *Macromol. Mater. Eng.* 294, 281–286 **(2009)**.

36. J. Bandyopadhyay and S. Sinha Ray, *Polymer* **(2010)** doi:10.1016/j.polymer.2010.01.029

37. S. Sinha Ray, J. Bandyopadhyay, and M. Bousmina, *Euro. Polym. J.* 44, 3133–3145 **(2008)**.

38. S. Sinha Ray and M. Bousmina, *Macromol. Chem. Phys.* 207, 1207–1219 (**2006)**.

39. Very roughly calculated using group contribution method of Fredor. Krevelen DWV. Properties of Polymer. Amsterdam, The Netherlands: Elsevier; 1990.

40. T. G. Mezger, The Rheology Handbook. Second Edition, Vincentz, Germany 2006.

Table 1. The parameters related to phase transitions of pure polymer and nanocomposites calculated from DSC thermograms

Sample	From 1st heating scan				During cooling from melt			From 2nd heating scan			
	T_g /°C	T_{m1} /°C	T_{m2} /°C	T_{m3} /°C	$T_{c,on}$ /°C	T_c /°C	ΔH_c J/g	$T_{m,on}$ /°C	T_{m2} /°C	T_{m3} /°C	ΔH_f J/g
PBSA	-43.8	44.9	81.9	94.1	69.0	56.8	47.5	18.9	83.1	94.5	56.6
PBSANC0.2	-44.0	44.4	82.9	93.6	69.5	56.5	48.4	22.0	82.4	93.7	56.5
PBSANC0.5	-43.3	44.4	82.9	93.6	69.5	56.8	47.6	21.7	82.7	94.0	55.9
PBSANC1	-43.6	44.6	82.9	93.2	69.7	56.3	47.3	22.0	82.2	93.6	56.5
PBSANC1.5	-43.7	44.4	82.2	93.4	70.7	55.9	45.3	21.2	82.2	93.8	57.0
PBSANC2	-43.5	44.6	83.4	94.4	71.0	54.4	45.3	22.9	82.7	94.8	53.6
PBSANC2.5	-43.9	44.9	81.0	93.4	70.5	54.7	44.8	25.5	82.4	94.0	52.1
PBSANC3	-43.5	46.1	81.7	93.2	70.2	55.1	44.6	26.2	82.2	93.7	52.4
PBSANC4	-44.6	45.1	81.0	92.2	70.2	55.0	45.0	26.7	80.7	92.8	52.0
PBSANC5	-43.7	46.1	80.7	92.9	70.2	54.4	44.0	28.4	81.0	93.2	52.0
PBSANC6	-44.0	44.6	80.5	93.2	70.0	53.7	42.3	28.6	80.5	93.5	49.6
PBSANC9	-44.4	45.6	78.8	92.2	70.2	52.4	41.7	28.6	79.5	92.8	49.3

The PBSA nanocomposites with various wt.% of C30B such as 0.2, 0.5, 1, 1.5, 2, 2.5, 3, 4, 5, 6, 9, were correspondingly abbreviated as PBSANC0.2, PBSANC0.5, PBSANC1, PBSANC1.5, PBSANC2, PBSANC2.5, PBSANC3, PBSANC4, PBSANC5, PBSANC6, and PBSANC9. T_g, glass transition temperature; T_{m1}, first melting peak; T_{m2}, second melting peak; T_{m3}, third melting peak; $T_{c\,on}$, crystallization onset temperature; T_c, crystallization peak temperature; ΔH_c, enthalpy of crystallization, $T_{m\,on}$, melting onset temperature; ΔH_f, enthalpy of fusion.

Table 2. The characteristic parameters of pure polymer and nanocomposites determined from amplitude sweep experiments

Sample	γ_L /% (corresponding to G')	γ_L /% (corresponding to G'')	γ_F /%
PBSA	6.81	14.67	–
PBSANC0.2	6.81	14.67	–
PBSANC0.5	6.81	14.67	–
PBSANC1	6.81	9.99	–
PBSANC1.5	4.64	6.81	–
PBSANC2	4.64	4.64	–
PBSANC2.5	2.15	2.15	–
PBSANC3	2.15	2.15	–
PBSANC4	1	1.47	–
PBSANC5	1	1	–
PBSANC6	0.15	0.46	3.16
PBSANC9	0.15	0.46	9.99

The PBSA nanocomposites with various wt.% of C30B such as 0.2, 0.5, 1, 1.5, 2, 2.5, 3, 4, 5, 6, 9, were correspondingly abbreviated as PBSANC0.2, PBSANC0.5, PBSANC1, PBSANC1.5, PBSANC2, PBSANC2.5, PBSANC3, PBSANC4, PBSANC5, PBSANC6, and PBSANC9. The parameters γ_L and γ_F, respectively, representing the yield strain of the LVE (liner viscoelastic range) range. i.e., the point from where the LVE plateau starts to deviate noticeably and the flow point where $G' = G''$ and the region between γ_L and γ_F is known as yield zone.

Table 3. The crossover point of moduli determined from frequency sweep experiments for pure polymer and nanocomposites

Sample	Coordinate of the crossover point, $G' = G''$
PBSA	(31.62, 105953)
PBSANC0.2	(31.62, 107642)
PBSANC0.5	(31.62, 102440)
PBSANC1	(31.62, 99538)
PBSANC1.5	(31.62, 102650)
PBSANC2	(31.62, 100561)
PBSANC2.5	(31.62, 105652)
PBSANC3	(17.78, 83982)
PBSANC4	(17.78, 88049)
PBSANC5	(1.78, 30488) – (1, 22780)
PBSANC6	–
PBSANC9	–

The PBSA nanocomposites with various wt.% of C30B such as 0.2, 0.5, 1, 1.5, 2, 2.5, 3, 4, 5, 6, 9, were correspondingly abbreviated as PBSANC0.2, PBSANC0.5, PBSANC1, PBSANC1.5, PBSANC2, PBSANC2.5, PBSANC3, PBSANC4, PBSANC5, PBSANC6, and PBSANC9.

Table 4. The glass transition and melting onset determined from the temperature ramp tests under dynamic mechanical conditions for pure polymer and nanocomposites

Sample	T_g (from G'' peak)/°C	T_g (from $tan\ \delta$ peak)/°C	$T_{m,\,on}$ (from G'' plots)/°C
PBSA	-42.8	-39.4	34.2
PBSANC3	-41.9	-38.6	37.4
PBSANC4	-41.8	-38.3	37.2
PBSANC5	-42.1	-38.7	37.2
PBSANC6	-41.7	-38.3	37.4

The PBSA nanocomposites with various wt.% of C30B such as 0.2, 0.5, 1, 1.5, 2, 2.5, 3, 4, 5, 6, 9, were correspondingly abbreviated as PBSANC0.2, PBSANC0.5, PBSANC1, PBSANC1.5, PBSANC2, PBSANC2.5, PBSANC3, PBSANC4, PBSANC5, PBSANC6, and PBSANC9. T_g, glass transition temperature; $T_{m,\,on}$, melting onset temperature.

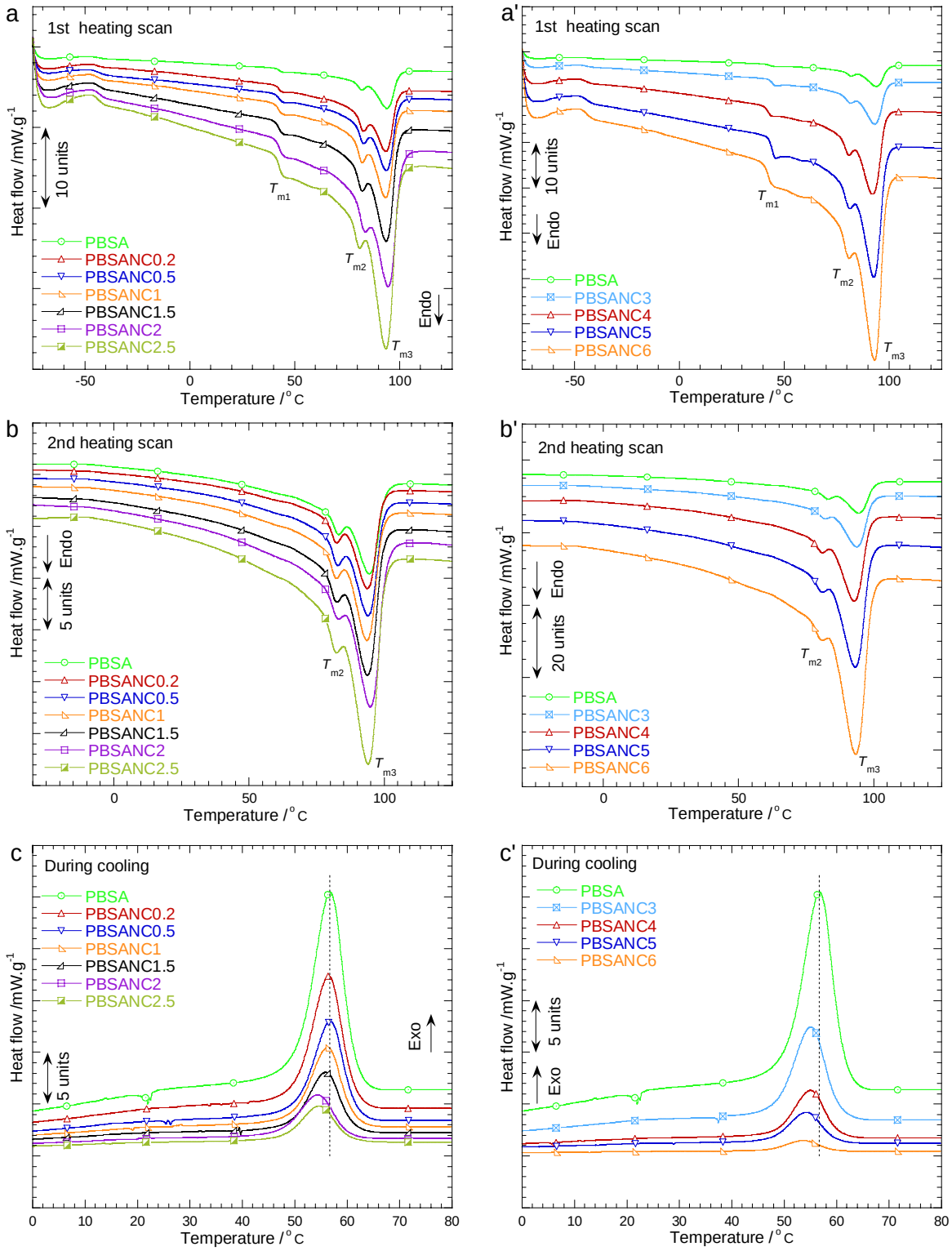

Fig. 1. Differential scanning calorimeter thermograms of pure polymer and various nanocomposite samples: (a, a′) first heating, (b, b′) second heating, and (c, c′) cooling from their melts. Heating-cooling-heating rate was 20°C/min. The PBSA nanocomposites with various wt.% of C30B such as 0.2, 0.5, 1, 1.5, 2, 2.5, 3, 4, 5, 6, 9, were correspondingly abbreviated as PBSANC0.2, PBSANC0.5, PBSANC1, PBSANC1.5, PBSANC2, PBSANC2.5, PBSANC3, PBSANC4, PBSANC5, PBSANC6, and PBSANC9.

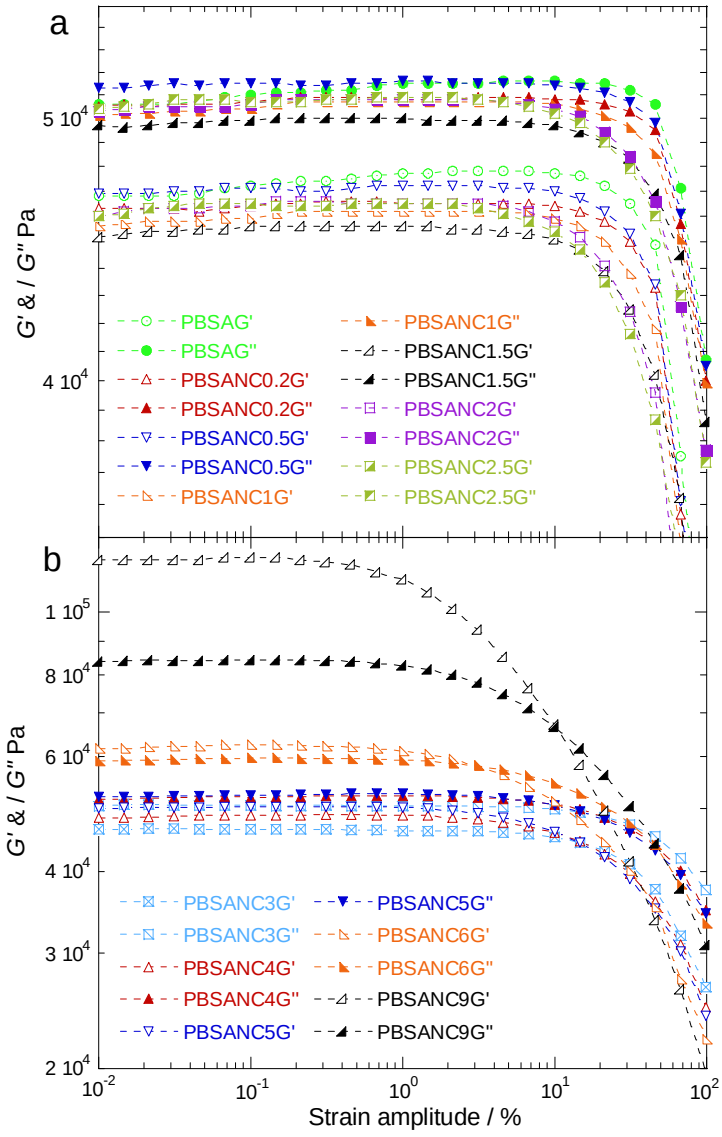

Fig. 2. The strain amplitude sweep experiments of pure polymer and various nanocomposite samples at 125°C with a constant angular frequency, ω =6.28 rad/s. Results show how the viscous behaviour of the neat polymer is changing to the gel behaviour in the case of nanocomposites with increase in clay loading. The PBSA nanocomposites with various wt.% of C30B such as 0.2, 0.5, 1, 1.5, 2, 2.5, 3, 4, 5, 6, 9, were correspondingly abbreviated as PBSANC0.2, PBSANC0.5, PBSANC1, PBSANC1.5, PBSANC2, PBSANC2.5, PBSANC3, PBSANC4, PBSANC5, PBSANC6, and PBSANC9.

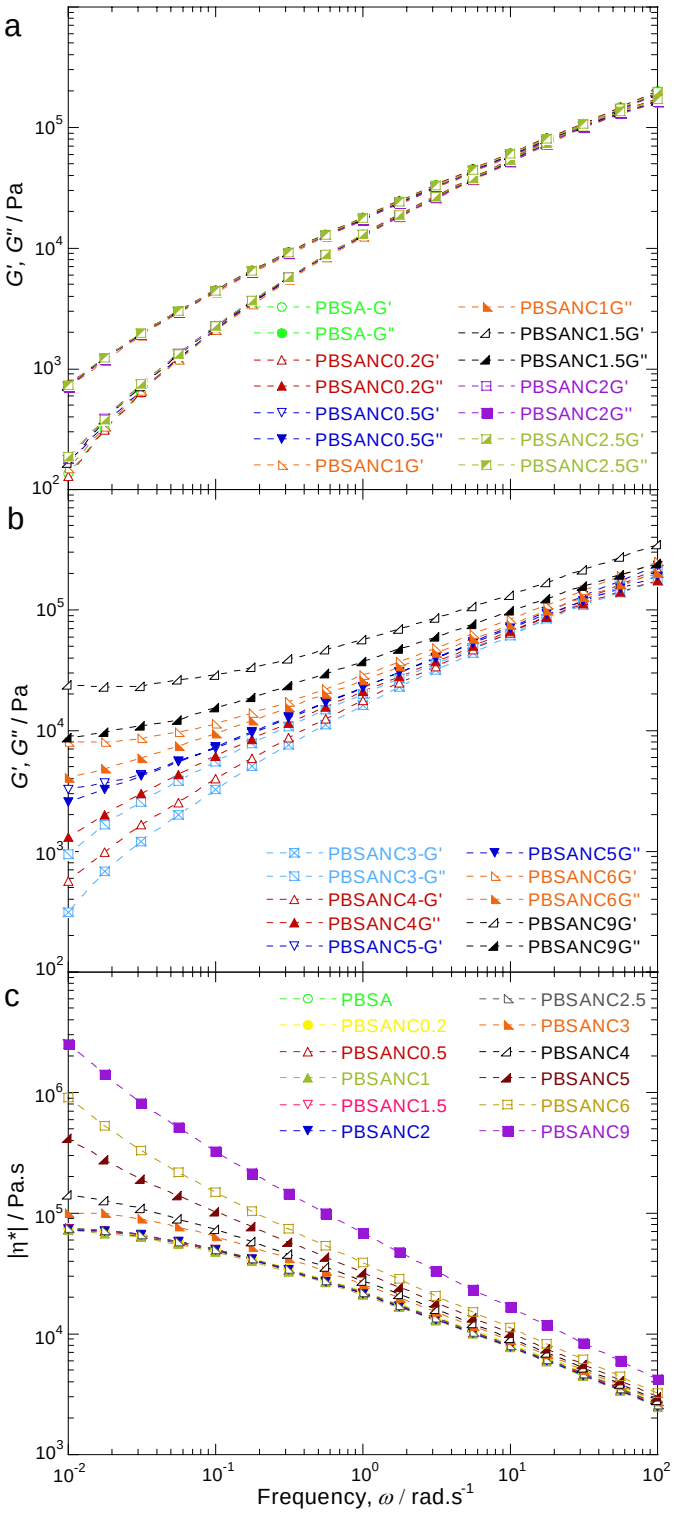

Fig. 3. The angular frequency dependence of storage modulus (G'), loss modulus (G'') and complex viscosity (η^*) of pure polymer and various nanocomposite samples. Frequency sweep experiments were conducted at 125°C with a constant strain value of 0.1%. The PBSA nanocomposites with various wt.% of C30B such as 0.2, 0.5, 1, 1.5, 2, 2.5, 3, 4, 5, 6, 9, were correspondingly abbreviated as PBSANC0.2, PBSANC0.5, PBSANC1, PBSANC1.5, PBSANC2, PBSANC2.5, PBSANC3, PBSANC4, PBSANC5, PBSANC6, and PBSANC9.

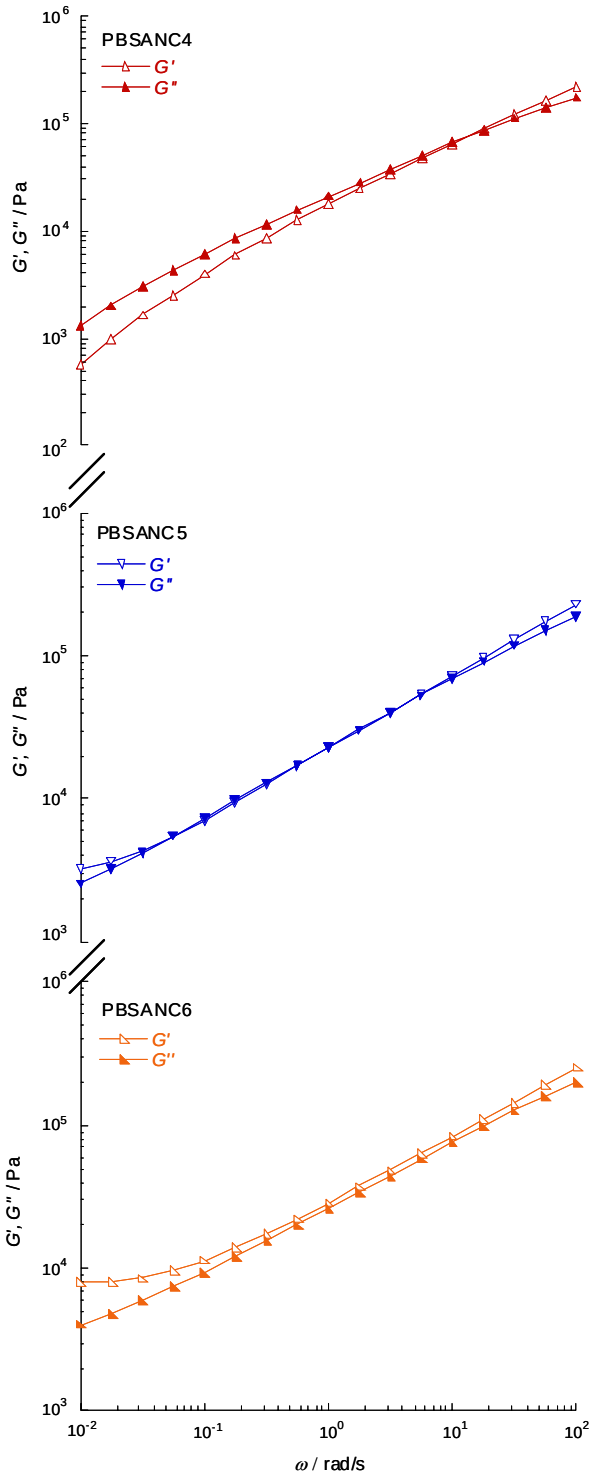

Fig. 4. Structural modification of nanocomposites with increase in C30B content from unlinked to sparsely cross-linked. The PBSA nanocomposites with various wt.% of C30B such as 4, 5, 6, were correspondingly abbreviated as PBSANC4, PBSANC5, and PBSANC6.

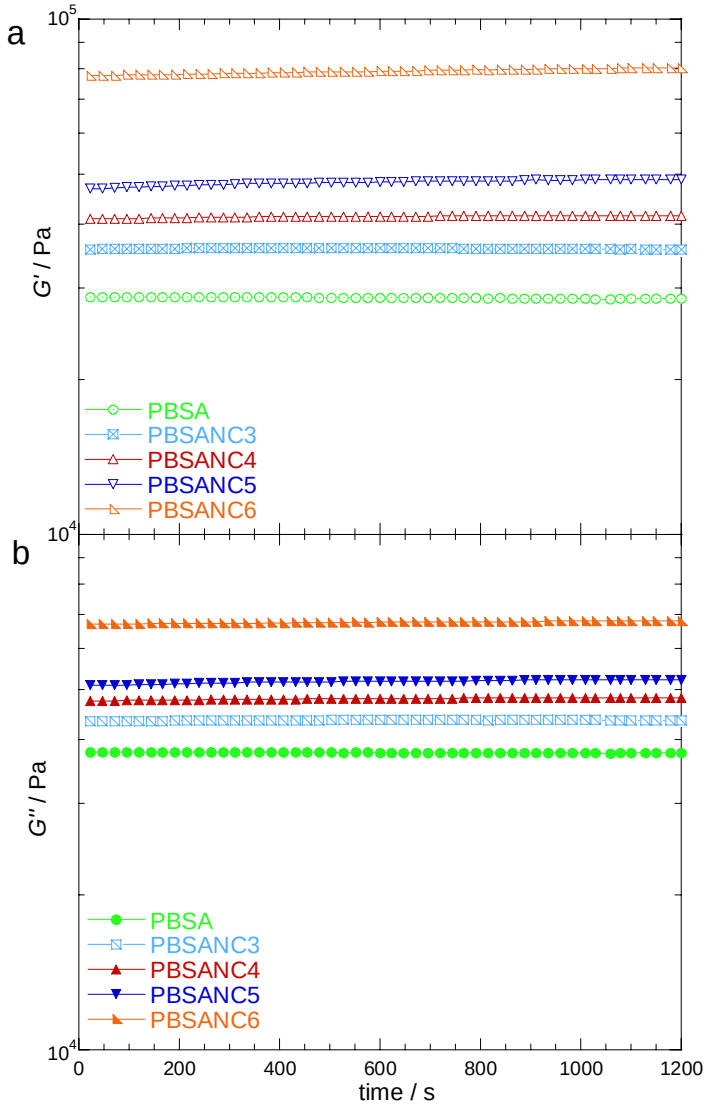

Fig. 5. The time dependence of storage modulus (G') and loss modulus (G'') of pure polymer and model nanocomposite samples. Time sweep experiments were conducted at 125°C with a constant strain and frequency value of 0.1% and 6.28 rad/s, respectively. The PBSA nanocomposites with various wt.% of C30B such as 3, 4, 5, 6, were correspondingly abbreviated asPBSANC3, PBSANC4, PBSANC5, and PBSANC6.

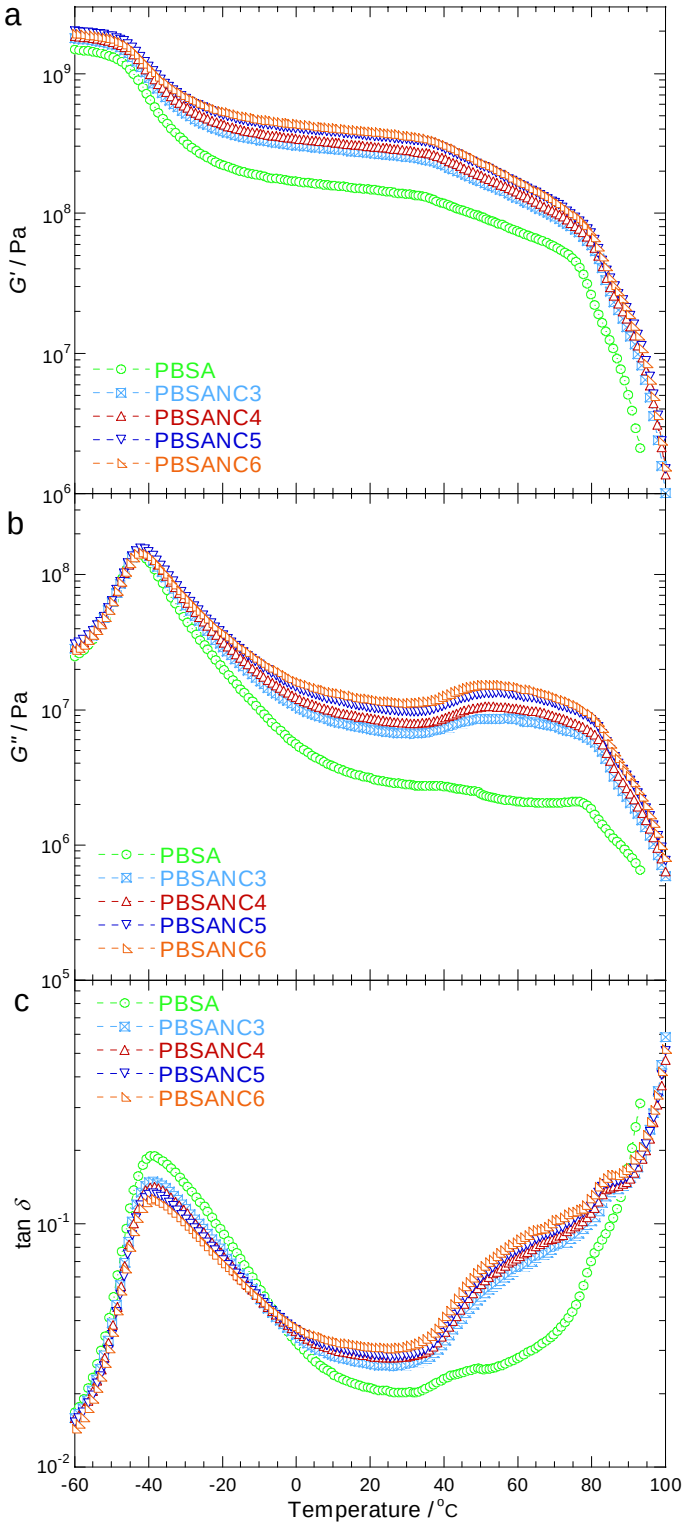

Fig. 6. Temperature dependence of storage modulus (G'), loss modulus (G'') and their ratio, $tan\delta$ of pure polymer and model nanocomposite samples. The PBSA nanocomposites with various wt.% of C30B such as 3, 4, 5, 6, were correspondingly abbreviated asPBSANC3, PBSANC4, PBSANC5, and PBSANC6.

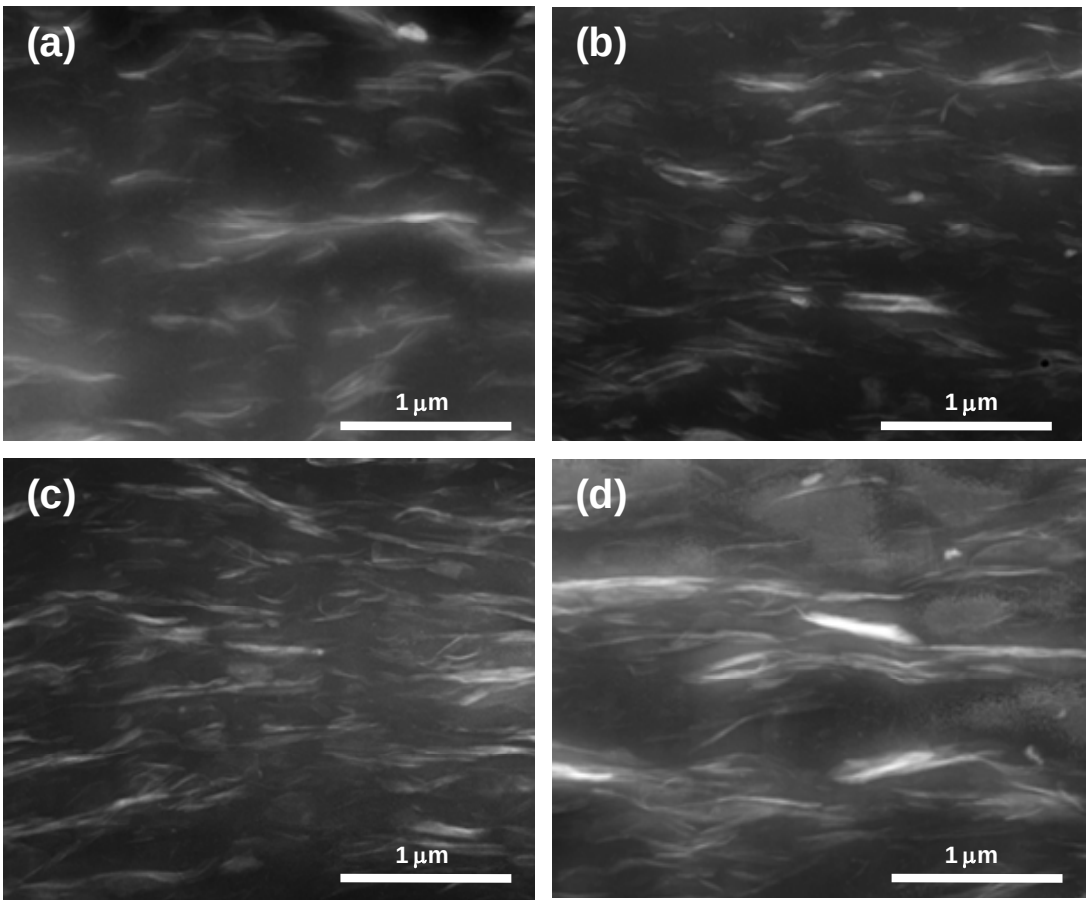

Fig. 7. The high-annular-angle-dark-field scanning transmission electron microscopy (HAAD-STEM) images of four different model nanocomposite systems, in which white entities represent the dispersed clay layers: (a) PBSANC3, (b) PBSANC4, (c) PBSANC5, and (d) PBSANC6. The PBSA nanocomposites with various wt.% of C30B such as 3, 4, 5, 6, were correspondingly abbreviated asPBSANC3, PBSANC4, PBSANC5, and PBSANC6.

Graphical Abstract

Thermal and Rheological Properties of Biodegradable Poly[(butylene succinate)-co-adipate] Nanocomposites

J. Bandyopadhyay, A. Maity, and B. B. Khatua, S. Sinha Ray*

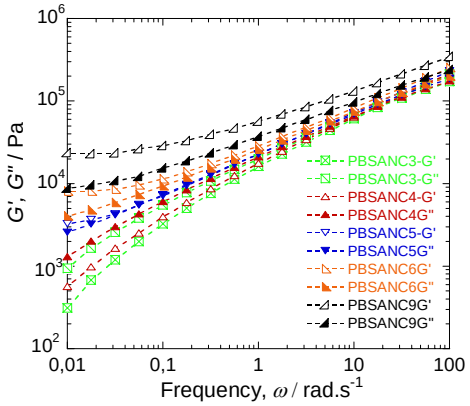

In this article we report on how the dispersion characteristics of the organically modified clay particles in the polymer matrix affects the thermal properties and flow behaviours of the nanocomposites. A series of poly[(butylenes succinate)-co-adipate] nanocomposites with various amounts of clay (0.2–9 wt.%) were prepared by melt-blending. Results show that the dominant viscous behaviour of pure polymer is getting suppressed up to a certain clay loading. Nanocomposite containing 5 wt.% OMMT is showing almost "at the gel point" behaviour, suggesting that the material is behaving near the borderline between liquid and solid; while nanocomposite containing 6 wt.% OMMT is showing the gel character. The dispersed structure of the clay particles in the polymer matrix was studied by scanning transmission electron microscopy.